Physics of the Earth and Planetary Interiors 170 (2008) 34–45

Contents lists available at ScienceDirect

Physics of the Earth and Planetary Interiors

journal homepage: www.elsevier.com/locate/pepi

Testing the robustness and limitations of 0–1 Ma absolute paleointensity data

L.B. Ziegler[a,*], C.G. Constable[a], C.L. Johnson[a,b]

[a] Cecil H. and Ida M. Green Institute of Geophysics and Planetary Physics, Scripps Institution of Oceanography, University of California, San Diego, 9500 Gilman Drive, La Jolla, CA, 92093-0225, USA
[b] Department of Earth and Ocean Sciences, University of British Columbia, 6339 Stores Road, Vancouver, B.C. V6T 1Z4, USA

ARTICLE INFO

Article history:
Received 18 December 2007
Received in revised form 8 July 2008
Accepted 10 July 2008

Keywords:
Paleointensity
Paleomagnetism
Geomagnetism
Paleomagnetic secular variation

ABSTRACT

Absolute paleomagnetic field intensity data derived from thermally magnetized lavas and archeological objects provide information about past geomagnetic field behavior, but the average field strength, its variability, and the expected statistical distribution of these observations remain uncertain despite growing data sets. We investigate these issues for the 0–1 Ma field using data compiled in Perrin and Schnepp [Perrin, M., Schnepp, E., 2004. IAGA paleointensity database: distribution and quality of the data set. Phys. Earth Planet. Int. 147, 255–267], 1124 samples of heterogeneous quality and with restricted temporal and spatial coverage. We accommodate variable spatial sampling by using virtual axial dipole moments (VADM) in our analyses. Uneven temporal sampling results in biased estimates for the mean field and its statistical distribution. We correct for these effects using a bootstrap technique, and find an average VADM of $7.26 \pm 0.14 \times 10^{22}$ A m^2. The associated statistical distribution appears bimodal with a subsidiary peak at approximately 5×10^{22} A m^2. We evaluate a range of potential sources for this behavior. We find no visible evidence for contamination by poor quality data when considering author-supplied uncertainties in the 0–1 Ma data set. The influence of material type is assessed using independent data compilations to compare Holocene data from lava flows, submarine basaltic glass (SBG), and archeological objects. The comparison to SBG is inconclusive because of dating issues, but paleointensity estimates from lavas are on average about 10% higher than for archeological materials and show greater dispersion. Only limited tests of geographic sampling bias are possible. We compare the large number of 0–0.55 Ma Hawaiian data to the global data set with no definitive results. The possibility of over-representation of typically low intensity excursional data is discounted because exclusion of transitional data still leaves a bimodal distribution. No direct test has allowed us to rule out the idea that the observed pdf results from a mixture of two distinct distributions corresponding to two identifiable intensity states for the magnetic field. We investigate an alternative possibility that we were simply unable to recover a hypothetically smoother underlying distribution with a time span of only 1 Myr and the resolution of the current data set. Simulations from a stochastic model based on the geomagnetic field spectrum demonstrate that long period intensity variations can have a strong impact on the observed distributions and could plausibly explain the apparent bimodality. Our 0–1 Ma distribution of VADMs is consistent with that obtained for average relative paleointensity records derived from sediments.

1. Introduction

Absolute paleointensity data are important constraints on our knowledge of the geodynamo. They allow the possibility of exploring how geomagnetic field strength has varied over Earth's history and are essential for providing appropriate scaling to both time-averaged and time-varying magnetic field models that extend beyond the historical record. Time varying field models on centennial and millennial time scales already exist (Jackson et al., 2000; Korte and Constable, 2005a), and have proved useful for studying prehistoric secular variation, but the extension of such models to million year time scales has not yet been accomplished. They will, however, be important in understanding low frequency field variations, and giving better context to observations of the current and historical field.

Magnetic field models, generally derived by fitting mathematical functions to globally distributed observations of field intensity and direction, are limited in spatial and temporal resolution by the quality and abundance of available data. An ideal data set would include time series of intensity and directional variations of the magnetic field at many geographically diverse locations. In reality, we have two types of data: spot recordings of absolute field

* Corresponding author. Tel.: +1 858 534 8119.
E-mail address: lziegler@ucsd.edu (L.B. Ziegler).

0031-9201/$ – see front matter © 2008 Elsevier B.V. All rights reserved.
doi:10.1016/j.pepi.2008.07.027

intensity, inclination, and declination found from magnetized igneous rocks and archeological objects, and time series of absolute inclination variations and relative intensity and declination variations from magnetized sediment cores. Field intensity data have been particularly sparse until fairly recently, and are still less abundant than directional data. Yet, with a gathering supply of absolute paleointensity data, modeling of field intensity variations on million year timescales should be possible—especially if these data can be used in conjunction with time series of relative intensity variations derived from sediment cores.

The SINT relative paleointensity stacks (Guyodo and Valet, 1996, 1999; Valet et al., 2005), which are formed by averaging some tens of globally distributed relative paleointensity records, have already hinted at interesting features of long term field variations worth further investigation—for instance intensity lows at excursions and the proposed sawtooth paleointensity pattern near reversals (Valet and Meynadier, 1993). However, these stacks are limited in that they utilize only relative paleointensity data to create the model of field variations. The two most recent SINT curves (SINT800 and SINT2000 spanning the past 800 ka and 2 Ma, respectively) have used absolute paleointensity data to scale the SINT curves to represent absolute variations in virtual axial dipole moment (VADM), but different scaling procedures resulted in significantly different estimates of the mean VADM for the Bruhnes chron (6×10^{22} A m^{2}and 7.5×10^{22} A m^{2}for SINT800 and SINT2000, respectively). The SINT curves also lack the predictive power of a mathematical model for the field: they cannot be expanded to geographic variability beyond that of an axial dipole field, cannot be downward continued to examine the field at the core mantle boundary (CMB), and are not easily differentiated to show rate of change in the field.

Using paleointensity data for modeling, or even for other more basic inferences about the field is not necessarily straightforward. For example, various authors have found conflicting estimates of the mean field strength (e.g. McFadden and McElhinny, 1982; Constable and Johnson, 1999; Selkin and Tauxe, 2000; Tauxe and Kent, 2004). Differing estimates are often caused by including data based on variable standards of reliability (as determined by uncertainty, laboratory methods, materials used, and other factors) or which cover different age ranges. Since the process of determining paleointensities is far from standardized, with new developments still frequent in this field, the debate over what data are reliable is unlikely to be resolved soon. As mentioned above, progress still needs to be made on how to use both relative paleointensity records and absolute paleointensity data together to create time varying field intensity models. Since each type of data has different sources of noise, we need to look at each data source in detail in order to assess how they can be used together most appropriately to produce paleointensity models.

Here, we assess the current global absolute paleointensity data set to characterize its statistics and to evaluate it for its use in future modeling. We first review the data that are currently available, and some possible drawbacks of the data set. Then we use statistical techniques to test the consequences of restricting the available data based on certain criteria. We look specifically at data from 0 to 1 Ma, where both absolute paleointensity data and relative paleointensity data are adequately distributed in space and in time to make field intensity modeling potentially viable.

2. Data

A number of absolute paleointensity compilations have been made over the past few decades and subjected to detailed analyses to determine the average dipole moment, and the statistical distribution of the observations. We follow a precedent established in the 1980s (McElhinny and Senanayake, 1982; McFadden and McElhinny, 1982) when data sets for the 0–50 ka time interval were considered separately from those spanning million year time scales. For the 0–1 Ma time scale we use absolute paleointensity data derived from igneous geological materials, typically lava flows, that acquire a thermoremanent magnetization. The primary data set chosen is the PINT03 compilation (Perrin and Schnepp, 2004). To facilitate comparisons of results from different material types we use a subset of the more abundant archeomagnetic and lava data set from the 0 to 50 ka Geomagia50 database, and our own compilation of data from submarine basaltic glass (SBG).

2.1. PINT03

The PINT03 database consists of 3128 globally distributed data from igneous and baked contact sources. More data have been published since this compilation, so it represents a minimum of igneous sourced data available at present. Perrin and Schnepp did not do quantitative analysis on the data compilation, citing some potential sources of biases in estimating paleointensity statistics with the currently available data (e.g. biased temporal and regional distributions of data, data quality variability) and the low density of data in time. However, for the 0–1 Ma time period there are 1124 data, and we feel that the number, temporal and spatial coverage (Fig. 1) are sufficient to justify some quantitative analyses. Beyond 1 Ma, both absolute and relative paleointensity data are less plentiful. We also investigate the influence of some of the previously mentioned potential sources of bias on the resulting field intensity statistics.

2.2. Geomagia50

The Geomagia50 database (Donadini et al., 2006) compiles globally distributed data from both lava flows and archeological objects with ages in the range 0–50 ka. We specifically look at the time interval 0–7 ka, since data are concentrated in this range (2793 archeological data and 311 lava flow data). The PINT03 database contains data from igneous sources only. Absolute paleointensities can also be determined from archeological objects. For the purposes of evaluating the 0–1 Ma field, adding archeointensity data to the PINT03 compilation provides additional data in the small time interval over which data density is already highest. For this reason, we stick to using only the PINT03 data compilation to evaluate the 0–1 Ma field, and only use Geomagia50 to compare paleointensity data from archeological and igneous sources. Since these two data sources have different mineralogies and cooling rates, they could potentially give different results. We also use this database as a source of 0–7 ka lava data in this comparison, as it is a more recent compilation and with more data in this time range than the PINT03 database. Fig. 2 shows the temporal and regional distributions of data from archeological and igneous sources with ages between 0 and 7 ka, plotted in the same fashion as Fig. 1. Some statistical analysis has already been done using this data compilation to test the correlation of data found from differing material types and laboratory methods (Donadini et al., 2007). A comparison with their findings is included in our discussion.

2.3. Submarine basaltic glass

Within the category of igneous sources, we can also compare SBG data and other lava flow data. SBG has a distinct fabric and cooling history, and so could potentially provide different results than other igneous data, and has sometimes yielded average field strengths which differ from those computed from other igneous data (Selkin and Tauxe, 2000; Tauxe and Yamazaki, 2007; Heller et al., 2002; Valet, 2003). The PINT03 data set contains only a handful of SBG data, but more data can be added (i.e. Bowles et al., 2006; Gee

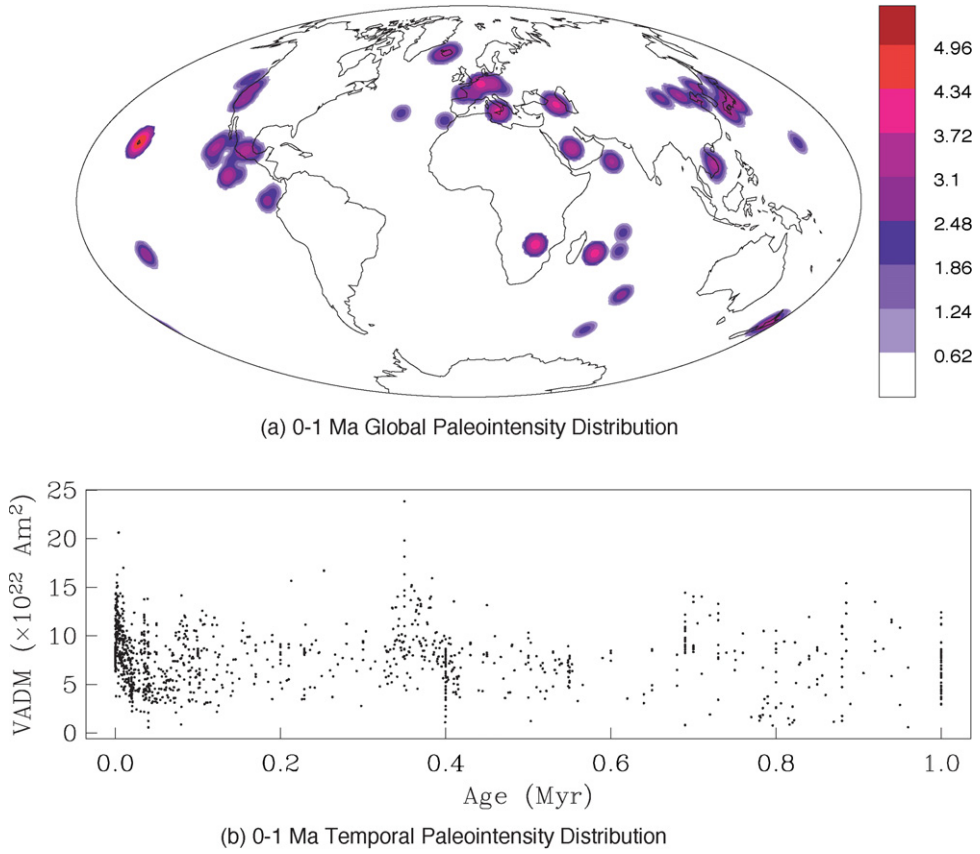

Fig. 1. (a) Global distribution of 0–1 Ma absolute paleointensity plotted as a probability distribution function on a log scale. Red (purple) values show areas with a high (low) concentration of data. Blank (white) areas have no data. (b) Paleointensity data are converted to VADM (see text) and plotted vs. age.

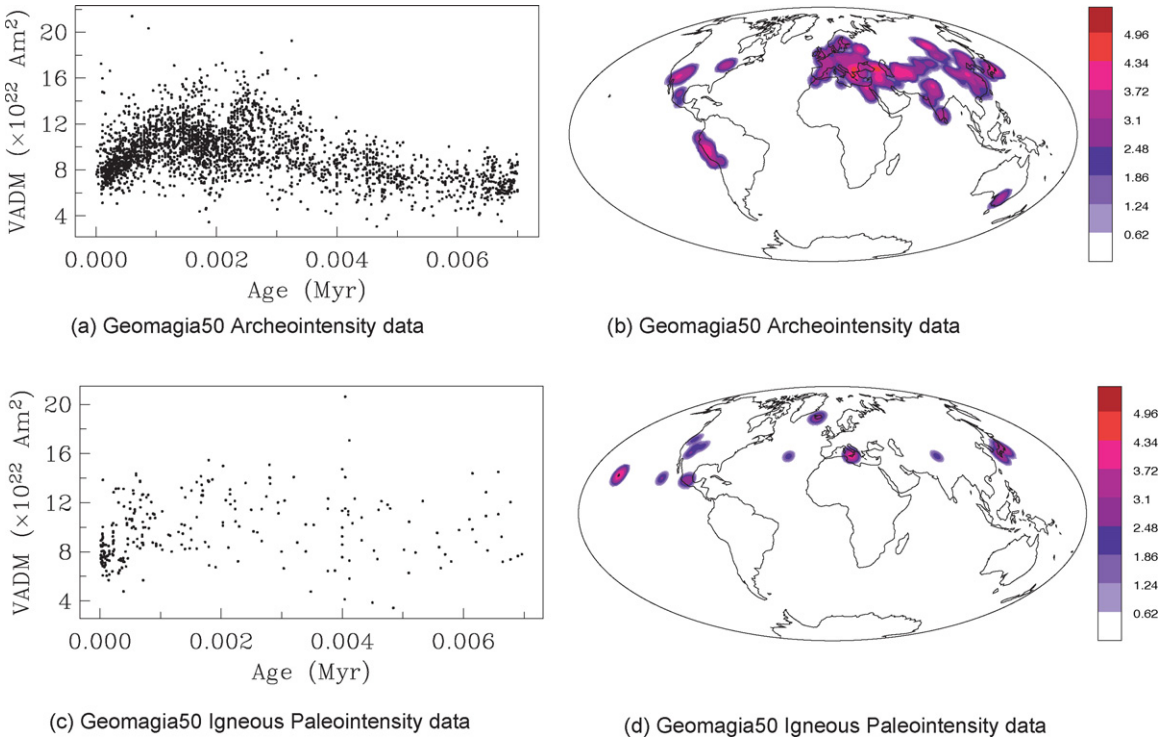

Fig. 2. Distribution of data from the Geomagia50 database with ages of less than 7 ky. (a) and (c) show distributions in time of data from archeological and igneous sources, respectively (with intensity converted to VADM). (b) and (d) show geographical distributions of data from archeological and igneous sources, respectively (format as for Fig. 1).

et al., 2000). Before mixing these material types into a larger compilation, results obtained from the different material types should be quantitatively compared. The SBG data used in this study are a compilation of data from (Bowles et al., 2005, 2006; Carlut et al., 2004; Carlut and Kent, 2000; Gee et al., 2000; Mejia et al., 1996; Pick and Tauxe, 1993) yielding 313 data all with nominal ages less than 100 ka based on crustal ages calculated from spreading rates and distances from the ridge axis. The actual ages are likely to be much younger than 100 ka (Bowles et al., 2006), and we discuss this later.

2.4. Potential drawbacks of the data set

Given that the Earth's magnetic field is predominantly dipolar, it is common to account for gross geographical variations in intensity data by converting to virtual axial dipole moments (VADM) (Barbetti, 1977). Temporal and spatial distributions of the PINT03 data are plotted in Fig. 1. The global distribution is plotted as a probability density function on the globe, with higher values (indicated by the pink end of the color spectrum) indicating higher data density. The time distribution is shown by plotting VADM vs. age. Data are unevenly distributed in time, with a high concentration of young data. A bias toward Northern hemisphere data is also clearly evident, as noted by Perrin and Schnepp (2004). Notably, over 512 data (almost half of the data set) are from Hawaii. In looking at global data sets of VADMs to calculate mean field strength, it is assumed that non-dipole components will be a source of noise, but contribute no bias in field statistics. However, if a large portion of data is from a single geographic region, the data compilation could potentially be biased toward reflecting any persistent non-dipole field components at that location (as shown by Korte and Constable, 2005b). To assess the accuracy of the assumption that the time averaged field is dipolar, we plot VADM vs. latitude (Fig. 3), along with the mean field strength (black line) and average VADM values for 15° latitude bins. If the dipole approximation is accurate, the time averaged VADM should be a constant, regardless of latitude. The bin averages show considerable scatter. Although this scatter could be attributed to non-dipole field effects, it is clear in Fig. 3 that a few bins contain data from very small time ranges, which is likely the source of scatter: that is, each bin average reflects the average VADM over different time ranges.

Besides the uneven temporal and spatial distribution, variable quality could also contribute to variance or bias in the currently available data set. The PINT03 database compiles all published data with no restrictions, but also contains fields of information which could be used to restrict data based on quality controls. One measure of data quality is the reported uncertainty in the paleointensity estimate, calculated as the standard deviation of the mean paleointensity of several specimens from a single cooling unit. However, paleointensity data are often only reported from a single specimen, in which case reported uncertainly is absent. Preferably, paleointensity estimates are made from more than one specimen, and have low reported uncertainty. Any reasonable restriction of this kind will significantly reduce the number of data.

Data quality can be checked or improved by employing laboratory methods which detect or minimize the potential for alteration. Paleointensity determinations could be inaccurate for this or other rock magnetic reasons. Several methods have been developed to specifically address these concerns, but debates over which methods are most appropriate still continue. Details of these topics are not discussed here; for more information see Tauxe and Yamazaki (2007) and Valet (2003). We note, however, that data obtained using the Thellier–Thellier method with pTRM checks (denoted T+ in the PINT03 intensity methods field) are often taken to be the most reliable, as they have built in heating steps which check for alteration. For this reason, we look at restricting the data by this criterion. An alternative method of guarding against data contaminated by alteration effects, the Shaw method, is not evaluated here, because of the small number of data in PINT03 gathered using this technique.

Finally, we note that the estimated ages of paleointensity data are often poorly constrained, with large or absent age uncertainties. This can be a big issue when looking at time-varying field intensity, and can also be an issue when looking at average field strength and investigating how methods, geographic bias, and materials may influence average paleointensity determinations. When comparing paleointensities from different geographic locations, materials, and methods, these paleointensities must be from the same time (or time span) so that differences in intensity results are not attributable to their simply sampling different field strengths.

3. Methods

We evaluate the 0–1 Ma absolute paleomagnetic data set with statistical methods, estimating the mean and variance as well as the probability distribution function (pdf) and empirical cumulative distribution function (ecdf). We use these properties to directly compare the original 1124 member data set with specific restricted subsets. Pdf estimation is done with an adaptive kernel method (i.e. kernel bandwidth varies with data density), using Abramson's square root law (Abramson, 1982) to determine bandwidth, as described by Silverman (1986). This non-parametric approach allows us to compare pdfs of subsets of data without imposing a potentially inappropriate parametric form. The empirical cdf (the probability that a value X will be less than or equal to x) is calculated directly from the data as a ratio of data less than or equal to x to total number of data, with linear interpolation to evaluate the function at evenly spaced values of x.

First, we need to address the uneven temporal distribution of the data. Since data concentration is heavily skewed toward young ages, our resulting statistics will be biased toward describing the recent field, instead of the 0–1 Ma field. If all paleosecular variation occurred with periods less than a few tens of kyr, it would not matter that the recent few kyr is so heavily represented, as it would not necessarily have a mean or other statistics which differed from a longer time range of data. However, long period variations are clearly evident in sedimentary relative paleointensity records (e.g. Valet et al., 2005). We cannot be sure that PSV with periods of longer than 1 Ma are not also occurring in the time varying field (see Section 5). Therefore, our results should be interpreted as describing the 0–1 Ma field only.

To correct for the uneven temporal distribution we use a variation of a bootstrap method (Efron and Tibshirani, 1993) to resample the original data set: we generate a set of n ages from 0 to 1 Ma randomly (with uniform probability) and from there choose from our original data set the paleointensity data whose ages most closely match each of the simulated ages as members of our new resampled data set. In this way, we bootstrap a distribution of n data from our original data set to create a resampled data set which is spread more evenly in time. We generate 1000 resampled sets of $n = 500$ data. Estimates of statistics do not change significantly with more than 1000 simulations (and actually converge with fewer simulations, so this is a conservative number). A mean VADM ($\bar{\mu}$) can be estimated by finding the average of the 1000 resampled means ($\bar{x}_i$). We can also calculate the standard error in the mean of $\bar{\mu}$, σ_μ. Variance $\bar{\sigma}^2$ and standard error of the variance σ_{σ^2} can be found analogously. Specifically, we calculate these

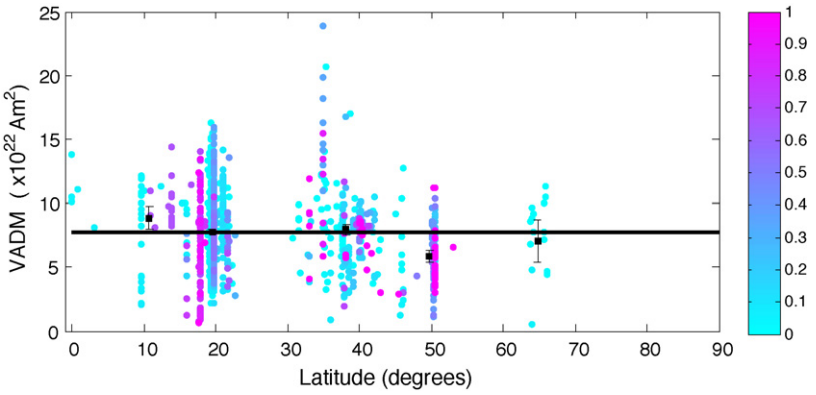

Fig. 3. PINT03 0–1 Ma VADM data plotted by latitude, and colored to correspond to age (circles). Color scale in Ma. Black squares are mean VADM values for 15°bins, with error bars showing 95% confidence bounds, calculated as 2× standard error in the mean. Black line is the average VADM for 0–1 Ma.

statistics using:

$$\bar{\mu} = \frac{1}{k}\sum_{i=1}^{k}\bar{x}_i \tag{1}$$

$$\sigma_\mu = \sqrt{\frac{1}{(k-1)}\sum_{i=1}^{k}(\bar{x}_i - \bar{\mu})^2} \tag{2}$$

$$\bar{\sigma}^2 = \frac{1}{k}\sum_{i=1}^{k}\bar{s}_i^2 \tag{3}$$

$$\sigma_{\sigma^2} = \sqrt{\frac{1}{(k-1)}\sum_{i=1}^{k}\left(\bar{s}_i^2 - \bar{\sigma}^2\right)^2} \tag{4}$$

where $k = 1000$, $\bar{s}_i^2$ is the variance of a resampled distribution, and the other variables are described above. Using this method, we not only attempt to correct for the uneven temporal sampling, but we can also find a reliable estimate on the error or stability of our estimate of mean and variance.

Fig. 4(a) and (b) shows histograms of the ages of the original 1124 data, and of one resampled data set. The resampled distribution has ages spread much more evenly in time. Fig. 4(c) illustrates this again by plotting the empirical cumulative distribution functions (ecdfs) of both data sets, along with the cdf of a uniform distribution for comparison. Since the 0–1 Ma data set has some gaps in time, we cannot truly create resampled data sets which are uniformly distributed in time. To test whether the temporal distribution of a typical resampled data set is distinguishable from a uniform distribution, we perform a Kolmogorov–Smirnov (KS) test, to quantify the difference between their ecdfs (see Press et al., 1986). We find a KS significance level of 0.61, where the level is on a scale of 0–1 with small values indicating a low probability that the samples come from the same underlying distribution. This test shows that the resampled distributions are not distinguishable from a uniform distribution. This technique eliminates bias generated by the high concentration of young data. Our results, discussed below, show that resampling significantly affects our estimated mean, variance and pdf. Therefore, we use this temporal resampling in all comparisons of the original data set to subsets based on restrictive criteria to make sure differences we see are not attributable to time-sampling issues.

4. Results

4.1. 0–1 Ma field statistics: temporal sampling effects

As shown in Table 1, the mean VADM of the original 0–1 Ma data set is $7.71 \pm 0.09 \times 10^{22}$ A m^2. Using our bootstrap procedure to simulate a temporally evenly distributed data set, the new estimate of the mean is $7.26 \pm 0.14 \times 10^{22}$ A m^2. A t-test confirms that we can reject the null hypothesis that these means are the same at

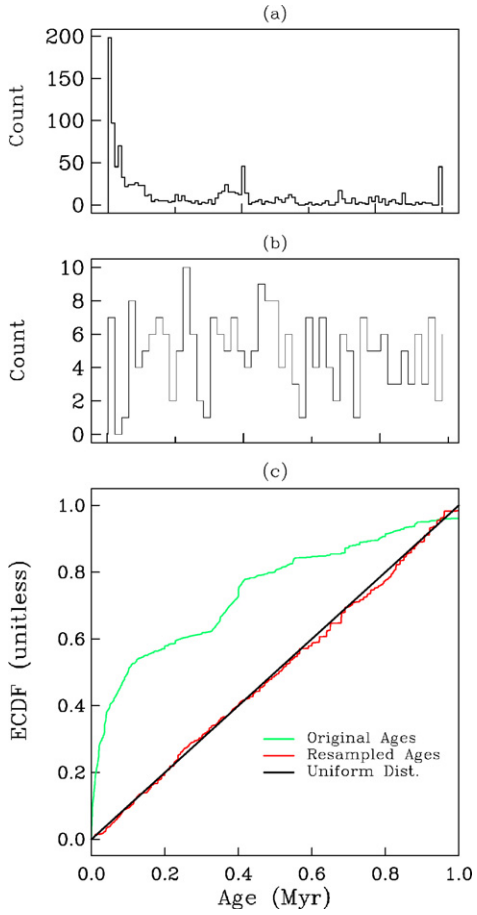

Fig. 4. (a) Histogram showing the age distribution of the 1124 0–1 Ma data from Pint03. (b) Histogram of the age distribution of a resampled set of 500 data (see text). (c) Ecdfs of the original Pint03 0–1 Ma data set (green), a resampled set of 500 data (red), and a uniform distribution (black).

Table 1
Statistics of data sets used in this study

	#	Mean	Variance	$\bar{\mu}$	σ_μ	$\bar{\sigma}^2$	σ_{σ^2}
All 0–1 Ma	1124	7.71	9.38	7.26	0.14	8.58	0.57
Low error	783	7.67	8.29	7.23	0.14	8.77	0.55
T+ only	874	7.60	9.59	7.16	0.14	9.73	0.63
T+ and low error	574	7.60	9.07	7.06	0.14	9.73	0.57
All 0–0.55 Ma	944	7.84	8.92	7.64	0.12	7.41	0.57
HI 0–0.55 Ma	508	7.84	8.43	7.29	0.13	7.57	0.57
No HI 0–0.55 Ma	436	7.83	9.64	7.68	0.15	11.41	1.18
Arch. 0–7 ka	2793	9.54	5.07	8.74	0.10	5.00	0.36
Lava 0–7 ka	311	9.56	6.02	9.77	0.14	6.41	0.55
Lava 0–7 ka cr*	311	8.31	4.55	8.50	0.13	4.87	0.42
SBG 0–100 ka[a]	313	8.33	7.74	–	–	–	–
SBG 0–10 ka[a]	158	9.40	2.61	–	–	–	–

is the number of data in data set, mean and variance are of the original data sets, $\bar{\mu}$ is the mean mean value of the bootsrapped distributions, σ_μ is the standard error in the mean, $\bar{\sigma}^2$ is the mean variance of the bootstrapped distributions, σ_{σ^2} is one standard error of the mean variance. All estimates of the mean and standard deviation of the mean are in units of ($\times 10^{22}$ Am^2), with estimates of variance and standard error of the mean variance in terms of the above units squared. cr* denotes the lava data after being adjusted for a hypothetical 15% high bias due to cooling rate. [a] Ages calculated as crustal ages (see text).

the $\alpha = 0.01$ level (i.e. if there were no difference, our observed difference would occur with a probability of less than 0.01). The lower mean is to be expected, since the procedure effectively reduces the influence of the higher than average young data. We also estimate the pdf and ecdf of the resampled data by averaging the 1000 distributions of data to find a mean distribution and 95% confidence bounds. These are plotted in Fig. 5(a) and (b), respectively. Looking at the estimated distributions in comparison to the originals, the significant changes can be identified by noting where the original distribution (black) lies outside the confidence bounds we have estimated (red dashed). In Fig. 5(a), some of the high VADM tail seen in the original distribution is absent in the mean resampled distribution. On the other end, the resampled data pdf shows more low VADM values. There is a sidelobe in the pdf around 5×10^{22} A m^2 which is not removed by accounting for the uneven temporal distribution.

4.2. An abundance of Hawaiian data

The spatial distribution of data is limited with a high concentration of northern hemisphere data. The distribution is too uneven to allow us to correct for its inadequacies as we have done for the temporal distribution. However, as mentioned above, 512 out of the 1124 data are from Hawaii. Only 4 Hawaiian data are older than 0.55 Ma. In the 0–0.55 Ma age range, 508 out of 944 data are from Hawaii. For this reason, we investigate the influence of Hawaiian data by comparing data from Hawaii only, data from everywhere but Hawaii, and the combined data set (Hawaiian and non-Hawaiian data) over the time range 0–0.55 Ma. We again simulate 1000 distributions of 500 data points for each data set. Results are shown in Table 1 and Fig. 5(c) and (d).

The bootstrapped mean for the Hawaiian data is slightly lower than that of the combined data set. However, the combined 0–0.55 Ma data set has a mean virtually identical to the data set without any Hawaiian data. Though at first glance it seems unexpected that the combined data set has a mean very similar to the non-Hawaiian data set despite the fact that the Hawaiian data has a lower mean than the non-Hawaiian data, this is clarified by looking at the medians for these distributions (which are often more robust estimates for the expected value of distributions which are non-gaussian). The estimated median of the combined data set (7.61×10^{22} A m^2) falls between the median of the Hawaiian data (7.35×10^{22} A m^2) and the median of the non-Hawaiian data set (7.80×10^{22} A m^2), as one would expect, and *t*-tests show that we cannot reject the null hypotheses that the means of the subsets are the same as the mean of the combined data set. This indicates that little bias is introduced to the combined data set by having such an abundance of data from one small region. However, the medians of the Hawaiian data and non-Hawaiian data are significantly different from each other ($\alpha = 0.02$), which could be due to persistent non-dipole field contributions at the Hawaii location. It is difficult to quantify how much of the small but statistically significant difference in mean and median values between these two subsets is due to non-dipole field components and how much of it is a time sampling issue, since simulating uniform time distributions with these smaller data sets becomes increasingly difficult (see Section 5).

Mean pdfs and ecdfs from the resampled distributions are plotted in Fig. 5(c) and (d). They are not significantly different from each other, except for a more pronounced sidelobe in the 'No Hawaii' data set. We do not show the confidence bounds in these figures for ease of viewing, but they overlap, confirming that differences among these three data sets are insignificant.

4.3. Restricting data quality

We next investigate whether higher quality data has different properties from the complete 0–1 Ma data set. As we already noted, there is still considerable debate over how to judge data reliability, and this is further complicated by the heterogeneous reporting of data and uncertainties. For now, we assess the influence of restricting the data based on reported error (reported errors must be either less than 20% or less than 5 μT for each result, with each result and reported uncertainty supposed to represent a cooling unit of a determined age), separately restrict the original data set to include only data produced using the Thellier–Thellier method with pTRM checks, and finally apply both of these requirements. Each subset of data spans the time range 0–1 Ma. Again, we resample 1000 distributions of 500 data points to estimate statistics and pdfs for each data set. Results are shown in Table 1 and Fig. 5(e) and (f).

Comparing $\bar{\mu}$ for each of these subsets to the $\bar{\mu}$ of the original data set, *t*-tests show we cannot reject the null hypothesis that they are the same ($\alpha > 0.05$ in each case). This result indicates that although including less reliable data in our estimates of field intensity statistics is not desirable, it does not significantly bias the results.

Pdfs for the various groups of observations are similar and all include the sidelobe seen in the complete data set, although the amplitude of the sidelobe varies for each data set. The subset of data which satisfy both the low error and Thellier–Thellier method with pTRM check criteria (green distribution in Fig. 5(e) and (f)) has a sidelobe with amplitude almost equal to that of the main peak.

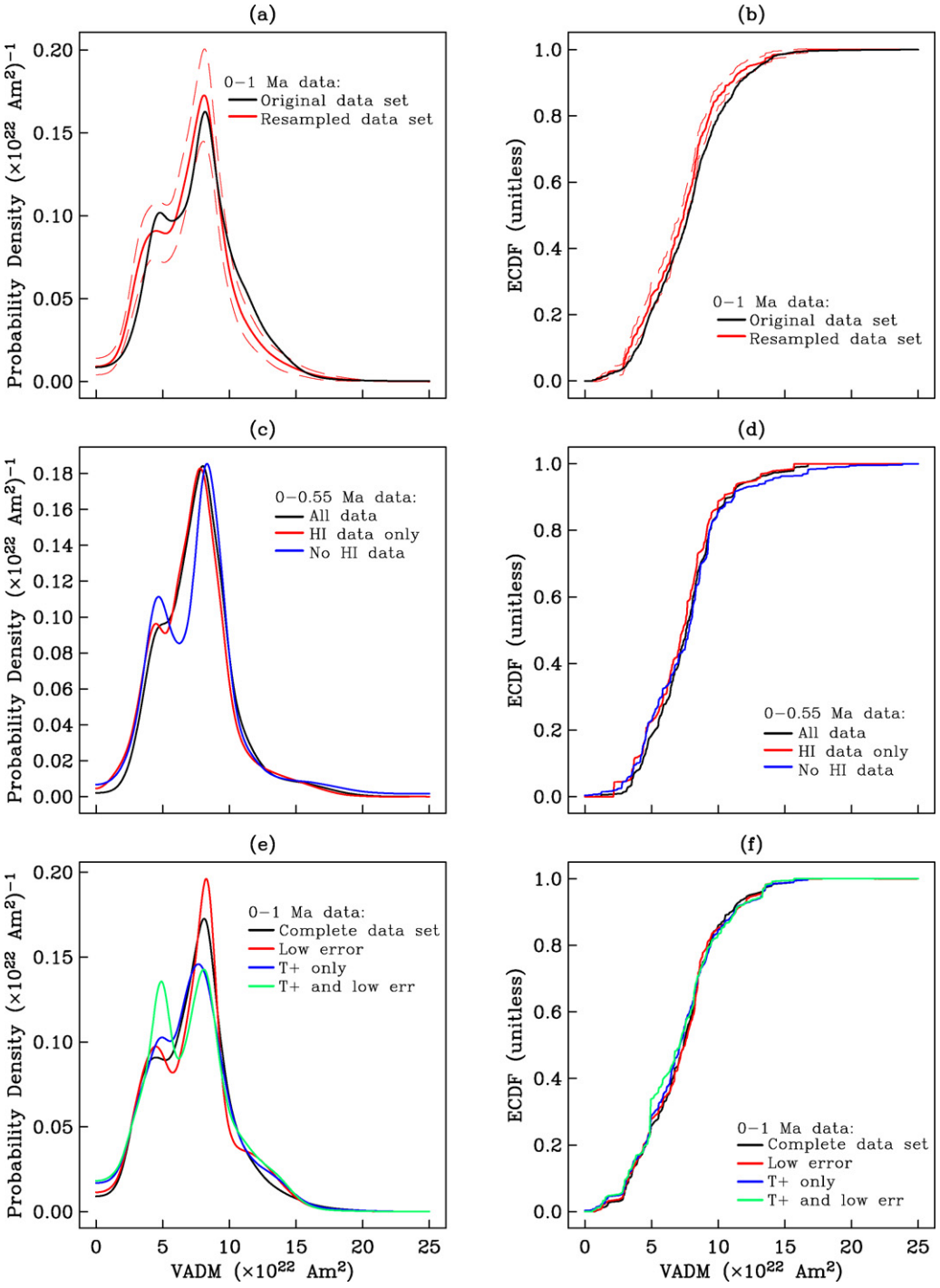

Fig. 5. (a) Pdf of the original 0–1 Ma Pint03 data set (black), the mean pdf of the 1000 pdfs of the resampled (temporally evenly distributed) data sets (red), and 95% confidence bounds of the mean pdf (red dash). (b) Ecdfs of original and resampled data with same color coding as (a). (c) and (d) Mean pdfs and ecdfs, respectively for the complete 0–0.55 Ma data set (black), Hawaiian data only (red), and all locations except Hawaii (blue). (e) and (f) Mean pdfs and ecdfs, respectively for the complete 0–1 Ma data set (black), data with reported errors less than 20% or 5μ T (red), data found using versions of the Thellier method with pTRM checks (blue), and data which are both reported to have low errors and which are found using Thellier methods with pTRM checks (green).

In this case, the exaggeration of the sidelobe is an artifact of our resampling procedure, which attempts to resample evenly in time, but runs into problems if large age ranges have little or no data. We find that there is a temporal gap for data meeting these strict requirements at around 0.6 Ma, and that on either side of the gap are data with values of about 5×10^{22} A m^2. Our procedure picks these two data points (on the edges of the gap) to represent the intensity over the entire time range of the gap in data, leading to an artificially large sidelobe at around 5×10^{22} A m^2. This issue is also evident in the lack of smoothness in the ecdf at the same VADM value: the sharp jump most likely is a result of a particular point or two being chosen many times for each resampled distribution. The effect this would have on the mean in this instance would be to bias it low (since 5×10^{22} A m^{2}is a lower than average VADM). Indeed, the mean of the highly restricted data set is lower (though not significantly lower) than that of the complete data set and the

subsets of data restricted based on method or reported error alone. Thus, the small differences between data sets in the investigation of using quality criteria restrictions reflect the limitations of the specific temporal sampling available rather than significant differences among the data sets themselves.

4.4. Influence of material type

4.4.1. Archeological vs. lava data

Compared to intensity estimates from igneous sources, archeointensity data may be more reliable. The mineralogy of archeological objects is generally more uniform (at least within site) than for igneous sources, and the magnetic carrier is more likely to be hematite in archeological objects, and so less prone to alteration during lab procedures. Additionally, archeological objects may cool more quickly (and uniformly within site) than lava flows, and so yield results less biased by large differences between the natural and lab cooling rates.

Here, we compare archeointensity data to paleointensities derived from igneous sources over the age range 0–7 ka (as compiled in Geomagia50). There are only 311 igneous paleointensities in this time range, compared to 2793 archeointensity data. Despite this, some meaningful comparisons can be made. Interestingly, the simple averages of VADMs of the two original data sets (without temporal resampling done) are almost identical. However, the picture changes after compensating for the uneven temporal sampling yielding a $\bar{\mu}$ of 8.74×10^{22} A m^2 for the archeointensity data set—significantly lower than the 9.77×10^{22} A m^2 obtained for the lava data set. We note that we have used $n = 300$ in the resampled igneous data distributions (instead of $n = 500$) due to the small size of the original data set. Igneous data have a higher variance both before and after correction for temporal sampling.

The mean pdfs and ecdfs of the corrected bootstrapped distributions (Fig. 6(a) and (b)) illustrate these differences. The igneous data pdf (black curve in Fig. 6(a)) is broader than the archeointensity pdf, and is offset to higher values of VADMs. Similarly the ecdfs in (b) (archeological data set in red, igneous in black) show the significant difference between the two data sets. This large difference merits further investigation (see Section 5).

4.4.2. Submarine basaltic glass

Some discussion has occurred about the reliability of SBG data (Heller et al., 2002; Valet, 2003; Tauxe and Yamazaki, 2007). Here, we attempt a comparison of SBG data to other igneous data and to archeointensity data over the same age range. However, this is not straightforward, as young SBG data are difficult to date. Many SBG data in our compilation have age estimates based on distance from the ridge axis (Mejia et al., 1996; Gee et al., 2000), so that the age corresponds to the crustal age, but is not necessarily the age of the uppermost lava flow which is being sampled. Bowles et al. (2006) derived ages using correlation with global paleointensity variations, but for this study we have recalculated these ages based on distance from the ridge axis and spreading rate to have an independent age estimate. Some studies have only restrictions on age (i.e. "less than 10 ka"), with no exact ages reported (e.g. Carlut et al., 2004; Bowles et al., 2005). Bowles et al. (2006), using paleointensities and geological features, showed that larger flows from the ridge axis and/or off-axis volcanism can lead to very young data (less than a few ka) derived from locations kilometers from the ridge. In this case, ages estimated by calculating crustal age based on spreading rates can be off by tens of kiloyears. Nominally, our SBG compilation ranges in age from 0 to 100 ka. However, the results of Bowles et al. (2006), indicate it is possible that the upper end of the range is much younger. To complicate the issue further, we cannot use our technique to resample evenly in time since the data ages are so uncertain. This is a real problem with the SBG compilation since data are heavily concentrated along the ridge axis.

To allow for these large uncertainties, we compared the SBG compilation to other data types in several age ranges, including lava data for 0–100 ka, 0–40 ka, and to lava data and archeointensities of ages 0–3 ka. By far, the best match in distributions for the SBG data is to compilations of paleo- and archeointensity data of 0–3 ka (Fig. 7(a)) (note that again, the subaerial lava data show some high paleointensites not seen in archeointensity data, although the effect is not as pronounced in this smaller data set). This supports the idea that data within a couple of kilometers of the ridge axis (which comprise the majority of this data compilation) are only a few 1000 years old, rather than sharing the crustal age of 20 ky. Data from Gee et al. (2000) and Bowles et al. (2006) are plotted vs. distance from ridge axis (Fig. 7(b)). These account for 237 out of 313 of the SBG data in our compliation. Comparing the pattern of SBG paleointensities vs. distance from the ridge axis to a plot of paleointensities (from other lava sources) vs. age in Fig. 7(c), the SBG paleointensities vs. distance plot looks like a stretched and truncated version of the paleointensity vs. age plot. This comparison further illustrates that ages of samples close to the ridge axis do not correlate well with crustal age.

The age uncertainties limit our ability to make conclusive detailed comparisons between SBG data and data from archeological objects or other igneous sources. It does seem clear that SBG samples give paleointensities comparable to those of other materials. We see no evidence that SBG paleointensities are biased low, as argued by some (Heller et al., 2002; Valet, 2003). If anything, the SBG data are high, though it seems clear that the high values are reasonable given the age uncertainty of the data.

5. Discussion and conclusions

5.1. Archeo- and paleointensity

Paleointensities determined from igneous sources are higher on average and have more scatter than archeointensities of the same age range (0–7 ka). The difference in means is a little over 10%. We considered two possible explanations for this. The first is that a systematic bias might arise from the laboratory methods used to determine paleointensity. From the Geomagia database it is straightforward to determine the general technique used (it is recorded for 88% of igneous and 83% of archeomagnetic results), and following an anonymous reviewer's comment that "it is well known that the microwave method yields lower determinations compared with the Thellier method" we assessed the relative distribution among Shaw, Thellier, and microwave methods in the two data groups. Only 1.5% of the archeomagnetic data were acquired using the microwave technique, compared with 14% of the igneous data. Thus the use of the microwave method can only be the source of bias if microwave paleointensities in this data set are systematically higher rather then lower than those from Thellier, Shaw and undocumented methods. We note that in general it is difficult to make systematic assessments of the influence of particular experimental methods because it is only in rare cases that direct comparisons have been made on identical samples.

A second explanation for the difference could be that lava flows and archeological objects have different natural cooling rates. It has been shown (Halgedahl et al., 1980; Dodson and McClelland-Brown, 1980; Fox and Aitken, 1980; Leonhardt et al., 2006) that when materials cool in nature at much slower rates than they do when cooling in laboratory paleomagnetic experiments, the paleointensities derived from the lab work can be biased high. If

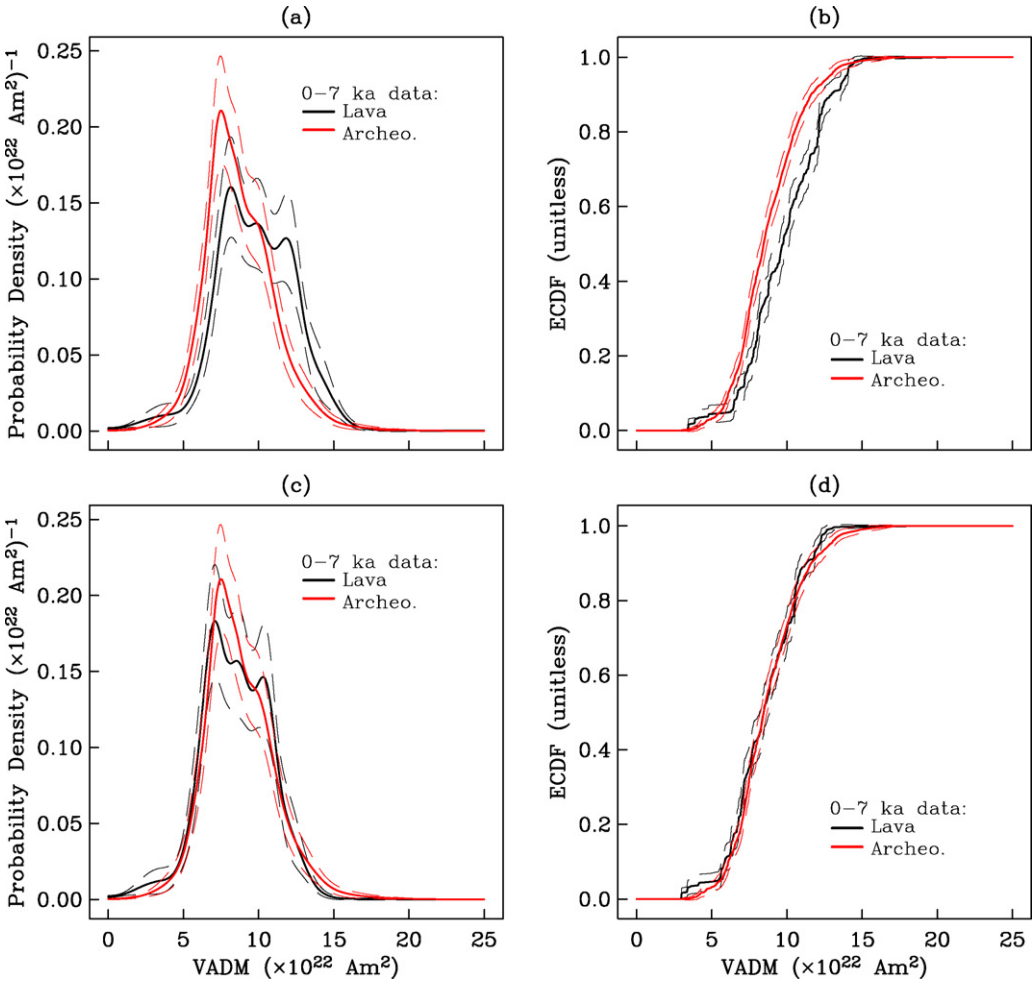

Fig. 6. Mean pdfs (a) and ecdfs (b) (as in Fig. 5) for 0–7 ka archeointensities (red) and paleointensities from lava flows (black). (c) and (d) Mean pdf and ecdf, respectively for archeointensities (red) and *adjusted* paleointensities from lava flows (black), for data whose ages of span 0–7 ka. Adjusted paleointensities calculated by reducing the actual paleointensities to account for a hypothetical 15% bias high due to lack of cooling rate corrections (see Section 5).

archeological objects cool more quickly in nature than lava flows, they would be less biased high than the lava data. While both materials likely have variable cooling rates from site to site, and so an exact correction cannot be applied to a global data set, we can test to see if the higher mean VADM for lavas (relative to archeointensity data) can be accounted for by a reasonably realistic cooling rate bias. If we assume that all paleointensities from igneous sources are 15% high (this easily falls in the observed range of cooling rate error) and adjust these data, the pdf and mean of the lava data look much more similar to those of the archeointensity data set (Fig. 6(c) and (d), Table 1). Of course, the archeointensity data could also be in need of a cooling rate correction (Fox and Aitken, 1980). However, as archeological objects generally cool more quickly and have higher blocking temperatures than lava specimens, they would incur less of a cooling rate error and need smaller corrections. Donadini et al. (2007) assessed the correlation among intensities derived from lavas and archeological objects, and found that the correlation was good (inferring from this that intensities derived from lavas are reliable), but the relationship between the two data sources was not 1:1, especially if considering only lava specimens which were analyzed using Thellier–Thellier method techniques. We do not test specifically for correlation, but also conclude that there is some discrepancy between the two data sets—enough to warrant more investigation and/or a correction factor but not enough to deem one source unusable.

5.2. Significance of sidelobe in PDF

In the original data set, we see an unusual sidelobe in the pdf of the VADM data set around 5 $\times 10^{22}$ A m^2. This feature did not disappear under any circumstances tested in this study.

The sidelobe could be due to typically low paleointensity transitional data (data which have virtual geomagnetic poles lower than a certain cutoff latitude—usually 45°, labeled 'T' in PINT03). We tested this by looking at a subset of 0–1 Ma data which specifically excluded transitional data. The sidelobe is still present.

Previous studies have noted bimodal distributions of virtual dipole moments (VDMs) for various time ranges and hypothesized that this might indicate two distinct states of geodynamo behavior (Heller et al., 2002, 2003). The structure in probability density we see in Fig. 5(a) appears somewhat more subtle than two distinct distributions. Additionally, we see no obvious two-state signal in the pattern of VADM vs. time (see Fig. 1b).

It is possible that the data set is not yet large enough to resolve a smooth pdf. However, it is also possible that the structure reflects some distinct property of geomagnetic field behavior, that could be resolved if we had a better understanding of how the magnetic field varies over time. To interpret the significance of the structure we see, we first investigate if a 1 Myr time series with the given temporal resolution (around 1000 data points per 1 Myr) is adequate to determine the underlying distribution associated with long term

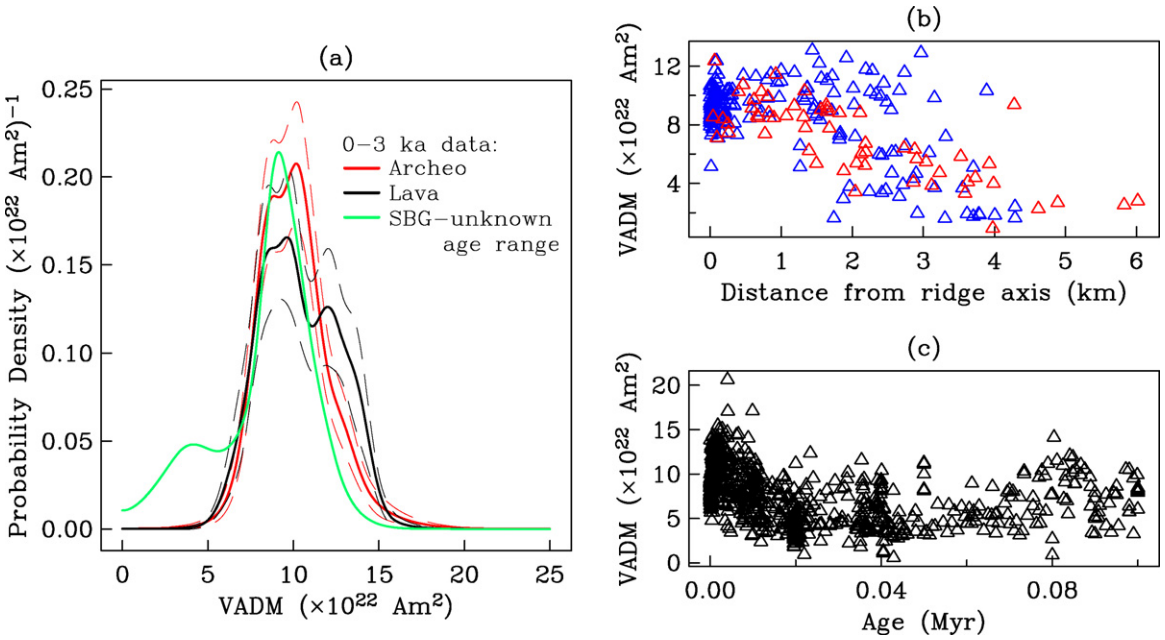

Fig. 7. Pdfs of archeointensities (red) and paleointensities from lava flows (black) as in Fig. 6 with ages spanning 0–3 ka, along with the pdf of SBG data (green) with ages spanning 0–100 ka as calculated by distance from the ridge axis,. Note that the pdf of SBG data is simply the pdf of our compilation of SBG data, not a mean pdf of resampled data sets. (b) SBG paleointensity data (converted to VADMs) from (Bowles et al., 2006) and (Gee et al., 2000) in blue and red, respectively plotted vs. distance from the ridge axis. (c) 0–100 ka paleointensity data from subarial lava flows (converted to VADMs) plotted vs. age.

paleofield behavior. For this purpose, we simulate time series which share the same spectral properties as paleomagnetic field intensity variations and then compare their statistical properties with those of our real data set. We model the spectral content using the paleomagnetic power spectrum for the dipole moment estimated by Constable and Johnson (2005) and shown in Fig. 8. For our tests we choose a simple functional form to approximate the empirical spectrum with a plateau at low frequency and a power law decay at high frequency. That is we suppose the spectrum $S(f)$ has the following functional form:

$$S(f) = \frac{a}{b + cf^{\mathrm{p}}} \tag{5}$$

and present specific results from the model function

$$S(f) = \frac{1}{1 + 0.005f^2} \tag{6}$$

The empirical paleomagnetic power spectrum and our model power spectrum are plotted together in Fig. 8. The simplistic model generally follows the trends of the empirical power spectrum. We make no attempt to derive a best fit model here, as it is not necessary for this exploratory exercise.

We simulate a 100 Myr time series of paleointensity data with the spectrum $S(f)$, and study the distributions of the 100 Myr record as well as 1 Myr subsets. The simulation has 1000 points per million years, to be comparable in data density to the 0–1 Ma absolute paleointensity data set. Fig. 8 shows an example of 1 Myr of simulated data and probability density distributions associated with the entire 100 Myr of simulated data as well as a few examples of 1 Myr distributions. Although the 100 Myr distribution is smooth and approximately normally distributed, we see a range of structures in the 1 Myr pdfs and variable levels of similarity to the 100 Myr pdf. One pdf agrees very well with the 100 Myr pdf, one has a sidelobe similar to the one we see in the real 0–1 Ma paleointensity distribution, and one has even more structure. This result indicates that we should not expect a time series with spectral properties of the paleofield intensity to be adequately represented by a 1 Myr time sample. Although the one million year samples have relatively similar means to each other and to longer time samples, 1 Myr is not long enough to recover the shape of the underlying distribution associated with field intensity. This simple experiment shows that we do not need to call upon two states of the geodyamo or other physical explanations to explain the structure we see in the 0–1 Ma absolute paleointensity data set.

Our interpretation of the sidelobe in the pdf for VADMs as a reflection of actual geomagnetic field behavior in the 0–1 Ma interval can be strengthened by supporting data from sedimentary relative paleointensity records. Fig. 9 shows the corresponding pdf derived from the most recent half of the SINT2000 dipole strength estimate (Valet et al., 2005), after re-normalization to the equivalent mean value. The sedimentary record (in gray) does indeed have a similar structure to the absolute intensity curve (black), but its variability is subdued in comparison. This is expected from the heavy smoothing that arises in temporal alignment and averaging of data from diverse sedimentary records. Such smoothing is well demonstrated by the power spectrum for SINT800 (Guyodo and Valet, 1999) which appears as the orange curve in Fig. 8. The power at frequencies higher than about 10–20 Myr^{-1} is attenuated substantially in SINT800 compared with other spectra derived from individual cores (brown, green, and blue curves), and corresponds to a reduced variance in the time domain. Individual relative paleointensity records derived from sediments might in principle provide a higher resolution pdf, but in our experience so far many of these are difficult to interpret directly because of the influences of varying sedimentation and other complicating factors.

5.3. *Suitability and limitations for field modeling*

The absolute paleointensity data set compiled in Pint03, including data from all laboratory techniques, reported error, and geographic locations can be used to evaluate average field behavior over the 0–1 Ma time range. The small variability in bootstrapped estimates of mean and variance indicate that the amount and quality of data provide robust estimates of these statistics. Our

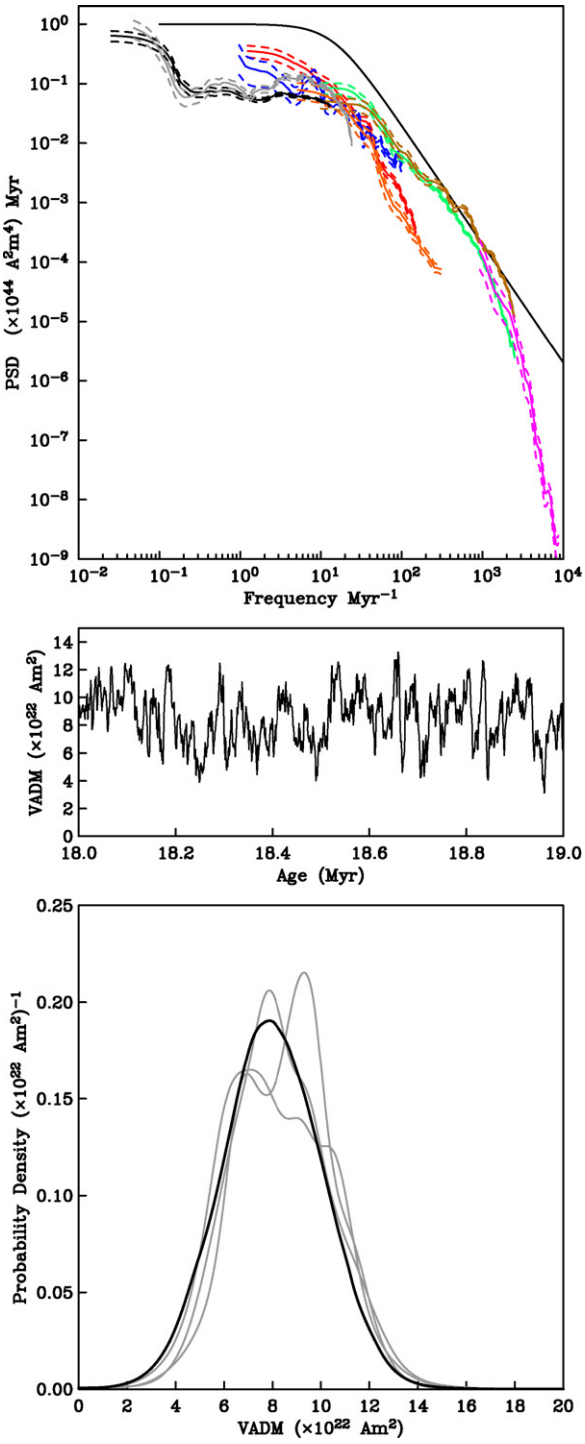

Fig. 8. (top) Empirical paleomagnetic power spectrum, reproduced from Constable and Johnson (2005) and model (heavy black). (middle) One million years of simulated paleointensity (see text). (bottom) Pdfs of entire 0–100 Myr simulated paleointensities (heavy black) and three pdfs of paleointensities from 1 Myr intervals (gray).

studies show that the mean VADM for the last million years is $7.26 \pm 0.14 \times 10^{22}$ A m^2. This result incorporates temporal resampling to correct for the uneven age distribution of the data. Further, the result changes only insignificantly when restricting the data used in the estimate to be of a certain reported uncertainty, to be obtained using Thellier–Thellier methods with pTRM checks, or to exclude data from Hawaii. This is reassuring, especially in the context of time varying field modeling, since it means that using lower quality data (and hence using a much larger data set) does not seem to greatly affect the resulting field.

Careful consideration will be needed when combining intensity estimates found from differing material types. Recent data from SBG, as compared to data from subaerial lava flows and archeological objects, seem to give comparable intensities. Detailed comparisons are difficult because of age uncertainties in very young SBG data. For young SBG data, the uncertainties in ages are too great to make the data useful for time varying field modeling, but for older samples the age uncertainties for SBG will be comparable to those in other materials. Nothing in this study indicated that young SBG data are biased to low values of VADM.

Further investigation into causes of observed differences in archeointensities and paleointensities derived from lavas will be necessary to find the most appropriate way to combine these data types in modeling. Differences in cooling histories between the two data sources could explain differences in mean intensities seen in our results, though we have not ruled out other reasons for the discrepancy between these two data types. The cooling rate explanation is significant because it would imply that lava data are biased to high values. A more detailed study of the differences would be useful in confirming our observations and finding more conclusive explanations.

One of the greatest limitations of the 0–1 Ma paleointensity data set is the poor spatial coverage, which restricts the capacity for any quantitative analysis in search of non-dipole signals and/or assessing their influence on field inferences based on the geocentric axial diople (GAD) assumption. Testing the GAD assumption would require (ideally) that data at each latitude (or in each latitude bin) cover the same time span, and that that time span is long enough and the data plentiful enough to be able to have a robust time-averaged field estimate at that latitude. In the small latitude range where these conditions are met (Fig. 3), the latitude bin averages are similar enough that adhering to the GAD assumption and converting data to VADM is not unreasonable. However, more investigation is needed and we can expect greater clarity on this issue as more data become available. An ongoing systematic analysis combining the absolute paleointensity data with relative paleointensity records from sediments should also help in this area.

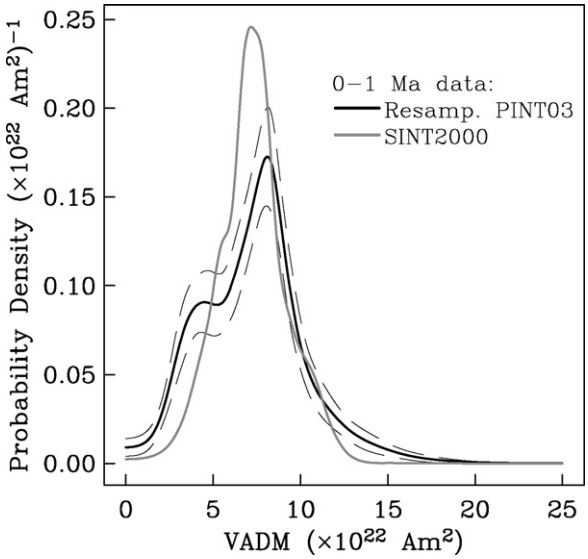

Fig. 9. Mean pdf of 0–1 Ma Pint03 resampled data sets (black) with 95% confidence bounds (black dash) identical to the red pdf in Fig. 5(a) and pdf of data points from the 0–1 Ma time interval of the SINT2000 relative paleointensity stack (see text).

Acknowledgments

This work was supported under NSF grants EAR-0337712 and EAR-0809709. We thank Lisa Tauxe, Kristin Lawrence, and Fabio Donadini for useful discussions. The text was improved by taking into account the comments of two anonymous reviewers.

References

Abramson, I.S., 1982. On bandwidth variation in kernel estimates—a square root law. Ann. Statist. 10 (4), 1217–1223.
Barbetti, M., 1977. Measurements of recent geomagnetic secular variation in Southeastern Australia and the question of dipole wobble. Earth Planet. Sci. Lett. 36, 207–218.
Bowles, J., Gee, J.S., Kent, D.V., Bergmanis, E., Sinton, J., 2005. Cooling rate effects on paleointensity estimates in submarine basaltic glass and implications for dating young flows. Geochem. Geophys. Geosyst. 6, Q07002.
Bowles, J., Gee, J.S., Kent, D.V., Perfit, M.R., Soule, S.A., Fornari, D.J., 2006. Paleointensity applications to timing and extent of eruptive activity, 9°–10° N East Pacific Rise. Geochem. Geophys. Geosyst. 7, Q06006.
Carlut, J., Cormier, M.H., Kent, D.V., Donnelly, K.E., Langmuir, C.H., 2004. Timing of volcanism along the northern East Pacific Rise based on paleointensity experiments on basaltic glasses. J. Geophys. Res. 108, B04104.
Carlut, J.C., Kent, D.V., 2000. Paleointensity record in zero-age submarine basaltic glasses: testing a new dating technique for recent MORBs. Earth Planet. Sci. Lett. 183, 389–401.
Constable, C.G., Johnson, C.L., 1999. Anisotropic paleosecular variation models: Implications for geomagnetic observables. Phys. Earth Planet. Int. 115, 35–51.
Constable, C.G., Johnson, C.L., 2005. A paleomagnetic power spectrum. Phys. Earth Planet. Int. 153, 61–73.
Dodson, M.H., McClelland-Brown, E., 1980. Magnetic blocking temperatures of single-domain grains during slow cooling. J. Geophys. Res. 85 (B5), 2625–2637.
Donadini, F., Korhonen, K., Riisager, P., Pesonen, L.J., 2006. Database for holocene geomagnetic intensity information, EOS Transactions. Am. Geophys. Union 87 (14), 137.
Donadini, F., Riisager, P., Korhonen, K., Kahma, K., Pesonen, L.J., Snowball, I., 2007. Holocene geomagnetic paleointensities: a blind test of absolute paleointensity techniques and materials. Phys. Earth Planet. Int. 161, 19–35.
Efron, B., Tibshirani, R.J., 1993. An Introduction to the Bootstrap. Chapman & Hall.
Fox, J.M.W., Aitken, M.J., 1980. Cooling-rate dependence of thermoremanent magnetisation. Nature 283, 462–463.
Gee, J.S., Cande, S.C., Hildebrand, J.A., Donnelly, K., Parker, R.L., 2000. Geomagnetic intensity variations over the past 780 kyr obtained from near-seafloor magnetic anomalies. Nature 408, 827–832.
Guyodo, Y., Valet, J.P., 1996. Relative variations in geomagnetic intensity from sedimentary records: The past 200,000 years. Earth Planet. Sci. Lett. 143 (1–4), 23–36.
Guyodo, Y., Valet, J.P., 1999. Global changes in geomagnetic intensity during the past 800 thousand years. Nature 399, 249–252.
Halgedahl, S.L., Day, R., Fuller, M., 1980. The effect of cooling rate on the intensity of weak-field TRM in single domain magnetite. J. Geophys. Res. 85 (B7), 3690–3698.
Heller, R., Merrill, R.T., McFadden, P.L., 2002. The variation of Earth's magnetic field with time. Phys. Earth Planet. Int. 131, 237–249.
Heller, R., Merrill, R.T., McFadden, P.L., 2003. The two states of paleomagnetic field intensities for the past 320 million years. Phys. Earth Planet. Int. 135 (2–3), 211–223.
Jackson, A., Jonkers, A.R.T., Walker, M.R., 2000. Four centuries of geomagnetic secular variation from historical records. Phil. Trans. Roy. Soc. Lond. A358 (1768), 957–990.
Korte, M., Constable, C.G., 2005a. Continuous geomagnetic field models for the past 7 millenia II: Cals7k. Geochem. Geophys. Geosyst. 6 (2), Q02H16.
Korte, M., Constable, C.G., 2005b. The geomagnetic dipole moment over the last 7000 years—new results from a global model. Earth Planet. Sci. Lett. 236, 348–358.
Leonhardt, R., Matzka, J., Nichols, A.R.L., Dingwell, D.B., 2006. Cooling rate correction of paleointensity determination for volcanic glasses by relaxation geospeedometry. Earth Planet. Sci. Lett. 243 (1–2), 282.
McElhinny, M.W., Senanayake, W.E., 1982. Variations in the geomagnetic dipole 1: the past 50,000 years. J. Geomag. Geoelectr. 34, 39–51.
McFadden, P.L., McElhinny, M.W., 1982. Variations in the geomagnetic dipole 2: statistical analysis of VDMs for the past 5 million years. J. Geomag. Geoelectr. 34, 163–189.
Mejia, V., Opdyke, N.D., Perfit, M.R., 1996. Paleomagnetic field intensity recorded in submarine basaltic glass from the East Pacific Rise, the last 69 ka. Geophys. Res. Lett. 23 (5), 475–478.
Perrin, M., Schnepp, E., 2004. Iaga paleointensity database: distribution and quality of the data set. Phys. Earth Planet. Int. 147, 255–267.
Pick, T., Tauxe, L., 1993. Holocene paleointensities: Thellier experiments on submarine basaltic glass from the east pacific rise. J. Geophys. Res. 98, 17949–17964.
Press, W.H., Teukolsky, S.A., Vetterling, W.T., Flannery, B.P., 1986. Numerical Recipes in Fortran 77: the Art of Scientific Computing. Cambridge University Press.
Selkin, P., Tauxe, L., 2000. Long term variations in palaeointensity. Phil. Trans. Roy. Soc. Lond. A358, 1065–1088.
Silverman, B.W., 1986. Density estimation for statistics and data analysis. Monographs on Statistics and Applied Probability. Chapman and Hall.
Tauxe, L., Kent, D. V., 2004. A Simplified Statistical Model for the Geomagnetic Field and the Detection of Shallow Bias in Paleomagnetic Inclinations: Was the Ancient Magnetic Field Dipolar? vol. 145, Geophysical Monograph. American Geophysical Union, Washington D.C., pp. 101–116.
Tauxe, L., Yamazaki, T., 2007. Paleointensities, vol. 5 Treatise on Geophysics. Elsevier, pp. 509–563.
Valet, J.P., 2003. Time variations in geomagnetic intensity. Rev. Geophys. 41 (1), 1004.
Valet, J.P., Meynadier, L., 1993. Geomagnetic field intensity and reversals during the last 4 million years. Nature 366, 234–238.
Valet, J.-P., Meynadier, L., Guyodo, Y., 2005. Geomagnetic dipole strength and reversal rate over the past two million years. Nature 435, 802–805.